Application of Lagrangian approach to generate P-I diagrams for RC columns exposed to extreme dynamic loading

Chunwei Zhang* and Masoud Abedini [a]

Multidisciplinary Center for Infrastructure Engineering, Shenyang University of Technology, Shenyang 110870, China

Abstract. The interaction between blast load and structures, as well as the interaction among structural members may well affect the structural response and damages. Therefore, it is necessary to analyse more realistic reinforced concrete structures in order to gain an extensive knowledge on the possible structural response under blast load effect. Among all the civilian structures, columns are considered to be the most vulnerable to terrorist threat and hence detailed investigation in the dynamic response of these structures is essential. Therefore, current research examines the effect of blast loads on the reinforced concrete columns via development of Pressure- Impulse (P-I) diagrams. In the finite element analysis, the level of damage on each of the aforementioned RC column will be assessed and the response of the RC columns when subjected to explosive loads will also be identified. Numerical models carried out using LS-DYNA were compared with experimental results. It was shown that the model yields a reliable prediction of damage on all RC columns. Validation study is conducted based on the experimental test to investigate the accuracy of finite element models to represent the behaviour of the models. The blast load application in the current research is determined based on the Lagrangian approach. To develop the designated P-I curves, damage assessment criteria are used based on the residual capacity of column. Intensive investigations are implemented to assess the effect of column dimension, concrete and steel properties and reinforcement ratio on the P-I diagram of RC columns. The produced P-I models can be applied by designers to predict the damage of new columns and to assess existing columns subjected to different blast load conditions.

Keywords: blast loads; damage index; Lagrangian method; P-I diagram; RC columns; vulnerability assessment

1. Introduction

Structures are able to mitigate the effects of explosions if they are analysed for most probable explosive detonation scenarios, and designed to sustain the effects for a desired scale of protection, taking into account both effectiveness and economy (Rezaei *et al.* 2020, Zhang *et al.* 2018). Therefore, the blast problem requires the identification of a number of considerations. Protection against explosives threats depends on the size of the explosive, the distance of the detonation relative to the structure, and the type of elements composing the structure (Mahdavi *et al.* 2019, Pandey 2010). Once they are identified, analysis is carried out using methods and techniques developed by engineers, and they vary from empirical methods which provide a considerable degree of conservatism, to advanced numerical methods which gives a close prediction to the actual behaviour. From all construction materials, concrete is employed and preferred in protective systems, because it encompasses fair characteristics in blast-resistance (Hadianfard and Farahani 2012). This corresponds to its popularity to be used in several civil structures for ordinary purposes, as it provides enormous benefits. Concrete is good in compression but weak in tension. Its stress-strain curve is nonlinear and changes with the change of loading condition. While steel is good in both tension and compression. Joining them results in reinforced concrete which has good flexure as well as axial and shear forces resistance characteristics.

The evaluation of deformations and damage resulting from blast loading is of great importance (Alipour *et al.* 2014, Jain and Chakraborty 2018). In general, the blast problem is complex because it requires the consideration of many factors that affects the applied loading and the material response (Alipour *et al.* 2015, Gang and Kwak 2017). Analysis methods of structural elements, including reinforced concrete elements, including columns, under blast load effects have been developed relatively by small group of scientists and engineers (Abedini and Zhang 2021). Early attempts of analysis methods started with experiments to capture the behaviour of the different elements, and then extended to include tests and trial and error construction to find the best solutions. These were conducted by means of small-scale prototype. In this method, proper effective parameters are selected and results are analyzed, then statistical regression method is applied to obtain empirical design and analysis equations and charts (Kim *et al.* 2018). This method gives excellent prediction for the behaviour of under blast; in contrast, it is costly and designed for only certain cases.

---

*Corresponding author,
Ph.D., Chair Distinguished Professor,
E-mail: zhangchunwei@sut.edu.cn
[a] Ph.D., Associate Professor, E-mail: m.abedini@sut.edu.cn

In addition to experiments, analytical methods by means of dynamic analysis procedures are used, in which forces and deformations are evaluated as a function of time. In these methods, the problem is formulated in the form of the equation of motion which considers time-dependent inertial forces. This will result in complex formulation added to the complexity of blast loading. Therefore, many methods were produced that simplify the blast problem by employing idealization to loading and material response. Of these methods, the single-degree-of-freedom (SDOF) is mostly used. The element in SDOF method is idealized to a simple vibratory system which can be analyzed using the principles of dynamic analysis. This method is afforded by many manuals which provide equations and graphs for solution. It is well suited to analyze simple structural elements and it gives conservative solution, but its drawback is its incapability to solve problems with higher degree of complexity and to capture the local damage in elements.

The finite element method is one of the powerful computational techniques resulted from the improvements in computational methods aided by computers. It has contributed a lot in solving complex systems including blast problems wherein computer is used and the fundamental laws of mechanics (the laws of mass, energy and momentum) as well used to properly introduce dynamic response in the material and the failure criterion using numerical techniques. The finite element method is widely used in blast applications because it has the ability to deal effectively with the geometrical, material and loading nonlinearities. There are many computer packages for finite element analysis which offer the modelling of blast problems, such as LS-DYNA which proved to have a reliable prediction of the local and general damage.

Traditional approaches of finite element method, Lagrangian and Eulerian, each has its own benefits and drawbacks. Lagrangian approach has been used widely in solid domains and Eulerian approach has been widely used in fluid fields. The Arbitrary Lagrangian Eulerian (ALE) formulation has emerged as a technique that can alleviate many of the shortcomings of the traditional Lagrangian and Eulerian formulations in handling these types of problems. The Eulerian approach is similar to studying the material particles from a constant position while the Lagrangian approach, is more like sitting on the particles and follows them while moving.

Pressure and impulse, as the two normalized parameters of a blast load, can be used to represent any blast condition. A P-I model is a design tool that allows of evaluating the damage level of structural components induced by blast loads. In each P-I model, three domains are recognized: an impulsive, a dynamic, and a quasi-static loading regime. The impulsive regime is characterized by short load duration where the maximal structural response is not reached before the load duration is over. The dynamic regime is characterized by the maximum response being reached close to the end of the loading regime. Lastly, the quasi–static regime is characterized by a structure having reached its maximum response before the applied load is
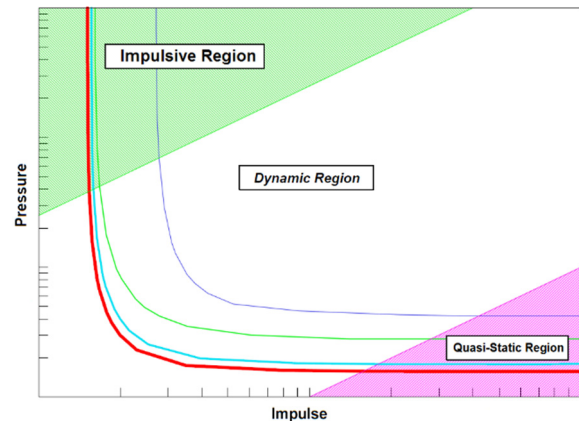

Fig. 1 Three regimes of loading

removed. The primary feature of P-I model is offered in Fig. 1 (Zhang *et al.* 2020).

Many researches work on the development of P-I model in columns subjected to explosive load have been published (Dragos and Wu 2013, Izman *et al.* 2015, Thiagarajan *et al.* 2013, Zhang and Abedini 2021). According to Abrahamson and Lindberg study (Abrahamson and Lindberg 1976), P-I model is used to assess the structural dynamic response. It illustrates that the combination of pressure and impulse produces an equal structure response. Cormie *et al.* (2009) presented three regimes of blast loading to generate P-I diagram based on the positive phase duration of blast loads, t_D and the natural period of the structure T. In the other study Li and Meng (2002) define P-I model as iso-damage curves which include three regimes of structural loading and response: impulse-controlled, peak load and impulse-controlled, and peak load-controlled regimes. In this study P-I diagrams for different RC columns are developed to study the effect of different parameters on the RC column dynamic responses, and to provide an efficient quantitative measure to assess the blast load resistance capacities of RC columns. In order to evaluate the behaviour of the RC column, three-dimensional finite element models have been developed using LS-DYNA. Validation study is performed based on the explosive test to investigate the accuracy of FE models to present the behaviour of the models. In the current research, Lagrangian methodology is generated for applying blast loads to columns in finite element models. A parametric study will be carried out to estimate pressure and impulse asymptotes (P_0 and I_0) in the RC columns when exposed to blast detonations.

2. Column models and geometry

The three-dimensional finite element meshes for all the RC columns are created in LSPREPOST software. The geometric modelling and meshing of concrete and steel bars was made using different elements types available in the software. The column is 500 × 700 × 4400 mm dimensions that presented in Fig. 2. In this study all the longitudinal reinforcement bars are assumed to have a circular cross section with a diameter ranging from 25 mm to 40 mm at
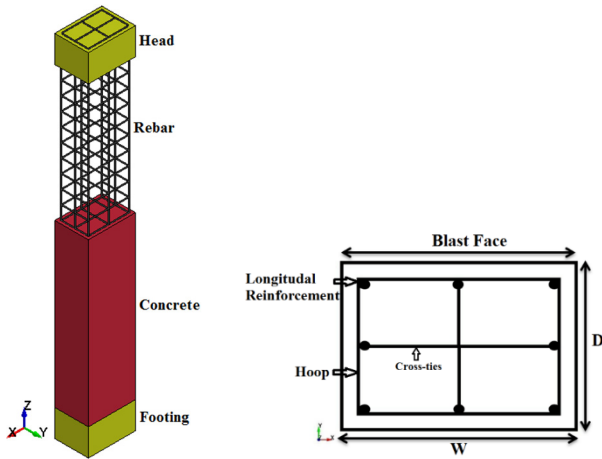
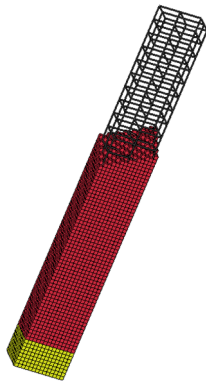Fig. 2 Isometric view of the column model in LS-DYNA

Table 1 Material properties of concrete and steel reinforcement

Material	Parameters	Value
Concrete	Uniaxial compressive strength	42 MPa
	Mass density	2400 kg/m^3
	Poisson's ratio	0.2
	Tensile stress at failure	6.0 MPa
Steel reinforcement	Young's Modulus	200 GPa
	longitudinal steel strength	460 MPa
	transverse steel strength	250 MPa
	Mass density	7800 kg/m^3
	Poisson's ratio	0.3
	Plastic strain at failure	0.18

Fig. 3 Longitudinal view of the column model in LS-DYNA

Node n_3, the reference node, determines the initial orientation of the beam cross section
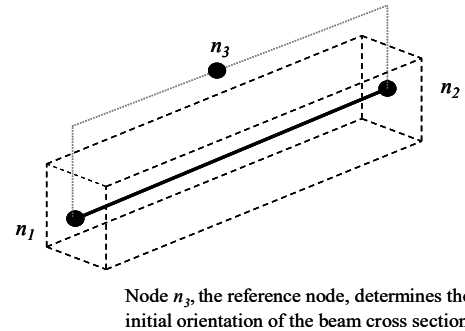
Fig. 4 LS-DYNA beam element (LS-DYNA 2007)

a spacing of 150 mm apart. Stirrups are modelled with 12 mm diameter at a spacing of 200 mm apart. A 50 mm cover space between concrete and steel rebar is assumed for all the models studied.

The reinforcement ratios of the RC column are as indicated in Fig. 3. The RC columns are supported at both ends which restricts the translational displacement of the columns at supports. The length of the support is 400 mm on each end at the bottom face and hence the effective column length is considered as 4400 mm between centerline of supports. The nodes of concrete solid elements at the support locations are restricted against translation as shown in Fig. 3 to simulate the actual test conditions. Table 1 gives the material properties of the concrete and steel reinforcement.

2.1 Element formulation

Two different types of elements are adopted in the study. They are solid elements to represent the concrete and beam elements to represent the steel reinforcement. In this study, 8-nodes constant stress solid elements with 1-point quadrature integration are employed to model the concrete members. The 2-node Hughes-Liu beam element with 2 × 2 Gauss quadrature integration is employed for modelling all the 460 MPa yield strength steel reinforcements. It has several desirable qualities such as being simple and robust,

yet results generated are compatible with the use of brick elements as its formulation is based on a degenerated brick element formulation. Each node of the created beam element has three rotational and three translational degrees of freedom (Zhang and Abedini 2022). Initial orientation of the beam element can be achieved by specifying a reference node as shown in Fig. 4. The beam element takes into account the axial, bending and torsional deformations, and is defined in LS-DYNA by using the keyword ELEMENT BEAM which requires the input of start point (N1), end point (N2), and nodal point (N3) to define the orientation of the principal r-s plane of the beam. This reference node must be unique for each beam element to prevent run time error. The position of the reinforcement elements is another factor that governs the size of the solid element for numerical modelling. In this study, the concrete meshes are established so that the reinforcement nodes coincide with the concrete nodes.

2.2 Material modelling

It is important to incorporate realistic material models to achieve a credible simulation of reinforced concrete structure, with appropriate physical parameters, into the finite element system. For this research, concrete and steel are modelled with the material models available in the commercial software LS-DYNA. Generally, the constitutive models require input parameters to develop several material relations such as tangential stiffness and failure surface

which are involved in the finite element analysis (Rashad and Yang 2019). These parameters include the basic concrete material properties such as the unconfined compression strength, the ultimate tensile strength, mass density in addition to other properties that vary from a model to another. The theoretical basis and features of these models are presented.

2.2.1 Concrete material model

Concrete is a composite material composed of a mixture of cement paste and aggregate, and provides fair characteristics in compression. The Material Model 72Rel3 in LS-DYNA developed by Karagozian & Case consulting engineering firm, is chosen due to its capability of reproducing the concrete behaviour under various stress conditions covering a number of important factors that are pertinent to the dynamic behaviours of concrete (Abedini and Zhang 2021b). This concrete model can give good estimation of the structure behaviour compared with the test results with its automatic generation. The K&C concrete damage model with its automated generation ability is normally used for modelling large scale structures with macro scale element sizes under impulsive load, i.e., blast or impact, and by default the localized width of damage is set equal to three times the maximum aggregate diameter. The failure of a RC structure under impulsive load is normally compression-dominated, because in such a structure the steel reinforcement would undertake most of the tensile forces even if damage occurs in concrete due to tension or shear.

In the last decade, many reinforced concrete models have been developed by researchers to determine the structural response when subjected to dynamic loading such as earthquake and blast loading. Some of the models proposed include Govindjee *et al.* (1995); Malvar *et al.* (1997); Lu and Xu (2004) and Wang *et al.* (2006). These concrete formulations can be categorized with regards to their damage function such as elasticity-based models, plasticity-based models, elasto-plastic damage models and plastic-fracturing models. Although these models have been proven to be highly satisfactory in estimating the structural response, further research in this field is still necessary in order to precisely define the complex behaviour of reinforced concrete.

It is necessary to consider both the uniaxial and triaxial stress states to construct the reinforced concrete material model accurately. To achieve this objective, precise failure criterion must be defined. Generally, concrete failure boundaries are defined as a region created by two surfaces namely the yield surface and the maximum failure surface in a three-dimensional principal-stress space as displayed in Fig. 5. From this figure, it can be seen that the maximum failure surface and yield surface are located in the principal stress space separated at some distance away from each other. Based on the findings from previous researchers, three failure modes can be identified when the concrete's loading surface intercepts the failure surface. The three failure modes are cracking, crushing and their combined effects.

For isotropic materials, like concrete, state of stress invariant functions is commonly used to develop the failure criterion and in this present study the concrete material failure criterion is defined by the stress invariants. With the stress tensor, σ_{ij}, the basic component of stress invariant functions is defined as the summation of two components namely deviatoric stress tensor, S_{ij} and hydrostatic stress tensor, $\sigma_h \delta_{ij}$. The general expression of δ_{ij} is as follows

$$\sigma_{ij} = s_{ij} + \sigma_h \delta_{ij} \tag{1}$$

and the pure hydrostatic stress is of the form

$$\sigma_h = \frac{1}{3}\left(\sigma_x + \sigma_y + \sigma_z\right) \tag{2}$$

where σ_x, σ_y and σ_z are the principal stresses in x, y and z direction, respectively. By rearranging Eq. (2), the deviatoric stress, or the pure shear state equivalent, can then be calculated using the expression.

$$s_{ij} = \sigma_{ij} - \sigma_h \delta_{ij} \tag{3}$$

Both deviatoric and hydrostatic components are crucial to the concrete model as they govern the behaviour of the material. In this case, the hydrostatic component has a significant influence on the strain hardening of the concrete material and the deviatoric component determines the behaviour of concrete when compressive failure is experienced.

For this concrete material the failure surfaces are constructed based upon the boundary created by the stress states. The simplest representation of the stress state at a point in failure surface of a three-dimensional stress space is illustrated in Fig. 6.

From this figure, the vector OB represents the state of stress interested in which it can be divided into two components: OA, the hydrostatic component which lies along the hydrostatic axis, and AB, the deviatoric component which lies on a deviatoric plane and this plane is
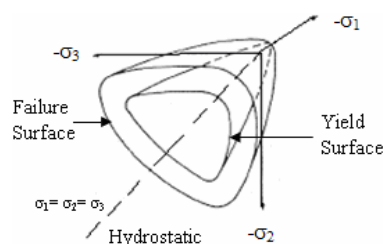
Fig. 5 Schematic failure surfaces of concrete material in three-dimensional stress space
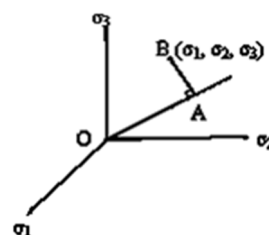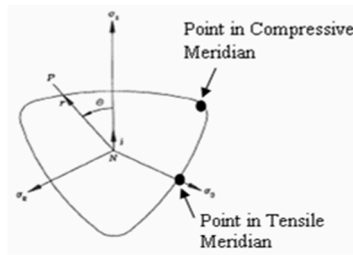
Fig. 6 Stress component in principal stress space

Fig. 7 Defining the deviatoric plane

perpendicular to the hydrostatic axis. Both the hydrostatic and deviatoric planes can be constructed by the extension of their respective axis.

With the assistance of these defined planes, the shape of the concrete failure surface can then be easily described with the stress meridians. The stress meridians of the failure surface are characterized as the intersection curves of the failure surface and the meridian plane which is a plane consisting of hydrostatic axis. To successfully develop the shape of the failure surface, two extreme meridian planes are needed and they are known as the compressive and tensile meridian. These two meridian planes are characterized as the meridian planes that are farthest and closest intersections from the hydrostatic axis respectively. Using these planes, the triangular shape failure surface is simply defined by a point in the compressive meridian and a point in the tensile meridian. The path between the extreme meridians is defined by an elliptical curve as displayed in Fig. 7.

This two-dimensional failure plane can then be extended to represent the concrete material failure surface cross sections in a three-dimensional space. This is achieved by defining the interaction of curves between the failure surface and the deviatoric plane. Using the defined failure planes, the initial yield surfaces, strength envelope and subsequent stress-strain relationships can then be constructed to model the crushing and cracking behaviour of the concrete material under loading (Abedini and Zhang 2021a).

The constitutive behaviour of concrete under the impact loading is best described by the stress strain relation as shown in Fig. 8. During the initial loading stage, the deviatoric stress components maintain within the elastic region until the stress state reaches the initial yield surface which will onset the weakening of the material under the increasing load. Damage of the material will not be observed until the stress state increases to the maximum surface. Any increase in load beyond this stage will result in either permanent plastic response of the material or
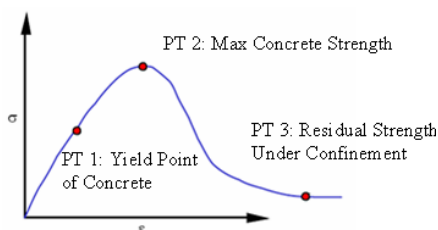
softening of material to a residual strength as shown in the figure.

Both concrete models employed in this study are developed with plasticity-based formulation with three pressure dependent failure surfaces as shown in Fig. 9.

The pressure on the failure surface of the concrete model is defined as

$$p = -\frac{1}{3}\left(\sigma_x + \sigma_y + \sigma_z\right) \qquad (4)$$

where both pressure and stresses are positive in compression. Hence the curves in Fig. 9 that are above the p axis correspond to the compressive meridians and vice versa for the tensile meridians.

As there is limited information regarding the material properties of the concrete, the self-generated concrete properties function offered by these two material models is used in the present study. In this case only the mass density and the unconfined concrete strength need to be specified into the computer program. LS-DYNA will then generate various concrete properties based on the unconfined concrete strength of the concrete material. These properties include the tensile strength of the concrete (f'_t), the cohesion strength of concrete, pressure hardening coefficient for the failure surfaces and the scaled damage parameters under compression and tension stated previously.

2.2.2 Steel material properties

In the current research material model Piecewise Linear Plasticity (material type 24) is used to simulate steel reinforcement in RC columns. This material model represents steel reinforcement behavior, with plastic deformation, strain rate effects, and failure. The advantage of this material model is that it allows an arbitrary stress strain curve and arbitrary strain rate dependency to be defined so that more accurate response can be acquired. The parameters for specifying the material properties of steel reinforcements are mass density, Young's modulus, Poisson's ratio, Yield strength and tangent modulus. The input parameters for this material model for longitudinal and transverse steel reinforcement are tabulated in Table 1.

2.3 Strain rate effect

The dynamic increasing factor (DIF) of concrete has
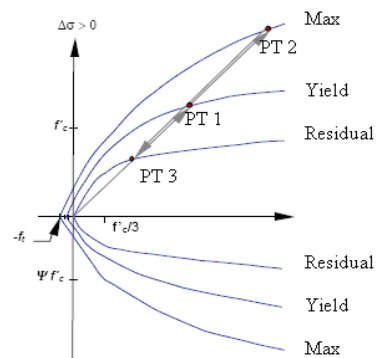

Fig. 8 Constitutive behaviour of concrete

Fig. 9 Failure surfaces of concrete

been a subject of extensive investigation and debate for many years. It is now generally accepted that the compressive DIF is attributable to the dynamic structural effect, whereas for concrete under tension the DIF is deemed to be governed by the material behaviour. Several manuals suggest values for the DIF. Proposed curves for a range of concrete strengths and steel yield and ultimate stresses are presented in TM 5-1300 manual, and they have been modified and updated in the UFC 3-340-02 manual, the manual latest release. These curves have patterns and features similar to the above cited curves. Also, the manual suggests selecting DIF is dependent on the following factors: pressure range or scaled distance to the explosion source, the type of stress, and finally the assumed degree of damage. However, the mechanisms governing the experimentally observed DIF remain to be a subject of much debate. The key issue is centralized about whether or not the DIF should be treated as an inherent material property, despite that in the widely-used CEB code (Comite Euro-International du Beton 1990) the DIF has been introduced as a material property. It tends to be generally accepted that under "uniaxial" compression, the DIF is rather a dynamic structural effect than a material property. Several recent studies have demonstrated that the inertia-induced radial confinement makes a large contribution to the dynamic compressive strength enhancement. When a high compression stress pulse is imposed to the specimen, the specimen tends to expand in the hoop direction, resulting in a radial inertia force which is equivalent to a confining stress, and subsequently increasing the axial strength of the concrete. As such, it is argued that the concrete DIF in compression should not be imposed at the material constitutive model level, i.e., it should be disabled or simply set as unity for material models that incorporate DIF for compression in a refined finite element analysis. On the other hand, when concrete is under tension, the radial inertia force would change direction; and moreover, the effect of lateral (inertia) stress on the axial tensile strength is very different from that of confining stress on the axial compression. As a matter of fact, the concrete tensile failure is much more localized than that under compression. Furthermore, experimental observations have indicated that the DIF for tension can be considerably larger than for compression at a comparable strain rate. Following equations can predict DIF for concrete and steel material models

$$CDIF = \frac{f_{cd}}{f_c} = \left[\frac{\dot{\varepsilon}}{\dot{\varepsilon}_{cs}}\right]^{1.026\alpha} \quad \text{for} \quad \dot{\varepsilon} \leq 30 \; s^{-1}$$

$$CDIF = \frac{f_{cd}}{f_c} = \gamma \left(\frac{\dot{\varepsilon}}{\dot{\varepsilon}_{cs}}\right)^{\frac{1}{3}} \quad \text{for} \quad \dot{\varepsilon} > 30 \; s^{-1}$$

(5)

$$TDIF = \frac{f_{td}}{f_{ts}} = \left[\frac{\dot{\varepsilon}}{\dot{\varepsilon}_{ts}}\right]^{\delta} \quad \text{for} \quad \dot{\varepsilon} \leq 1 \; s^{-1}$$

$$TDIF = \frac{f_{td}}{f_{ts}} = \beta \left[\frac{\dot{\varepsilon}}{\dot{\varepsilon}_{ts}}\right]^{\frac{1}{3}} \quad \text{for} \quad \dot{\varepsilon} > 1 \; s^{-1}$$

(6)

Where;

Compressive strength	Tensile strength
f_{cd} = dynamic compressive strength at $\dot{\varepsilon}$	f_{td} = dynamic tensile strength at $\dot{\varepsilon}$
f_c = static compressive strength at $\dot{\varepsilon}_{cs}$	f_{ts} = static tensile strength at $\dot{\varepsilon}_{ts}$
f_{cd}/f_c = compressive strength DIF	f_{td}/f_{ts} = tensile strength DIF
f_{cu} = static cube strength $= 1.205 \times f_c$	$\dot{\varepsilon}$ = strain rate in the range of 10^{-5} to 160 s^{-1}
$\dot{\varepsilon}_{cs}$= 30 × 10^{-6} s^{-1} (static strain rate)	$\dot{\varepsilon}_{ts}$= 3 × 10^{-6} s^{-1} (static strain rate)
$\dot{\varepsilon}$ = strain rate in the range of 1 to 300 s^{-1}	$f'_{co} = 10 \; MPa$
$log\gamma = 6.156\alpha - 0.49$	$\beta = 7.11\delta - 2.33$
$\alpha = \dfrac{1}{5 + \frac{3f_{cu}}{4}}$	$\delta = \dfrac{1}{10 + \frac{6f_c}{f'_{co}}}$

Steel is a critical component of reinforced concrete structures subjected to blast loads. The inelastic response of metallic materials to dynamic loading can be easily monitored and assessed due to the isotropic properties. From past experimental data, it has been found that the yield strength can almost be doubled for mild steel under high strain rates; the ultimate tensile strength can increase by about 50 % and the upper yield strength even higher. On the other hand, with increasing strain rate, the ultimate tensile strain decreases. Malvar (1998) provides a more detailed understanding of steel reinforcing bars under the effect of high strain rates. It has been observed that the failure strain for steel ranges between 13 to 20 percent. Hence, the failure criterion is based on the maximum principal strain criterion. Stress-strain curve for reinforcing steel can be seen in Fig. 10.

$$DIF = \frac{(\dot{\varepsilon})}{10^{-4}}^{\alpha} \tag{7}$$

Where

$$\alpha = 0.019 - 0.009 \frac{f_y}{414} \quad \text{for} \quad \text{ultimate stress}$$

$$\alpha = 0.074 - 0.040 \frac{f_y}{414} \quad \text{for} \quad \text{yield stress}$$

fy = steel yield strength

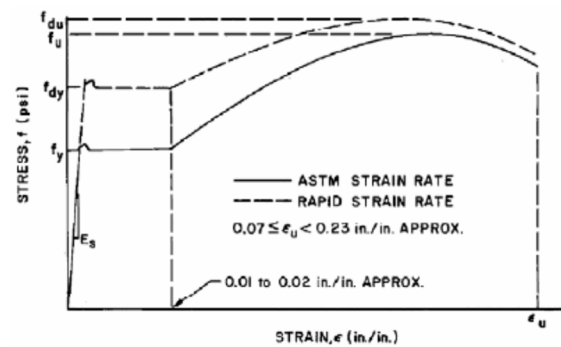$\dot{\varepsilon}$ = strain rate in the range of 0 to 225 s − 1
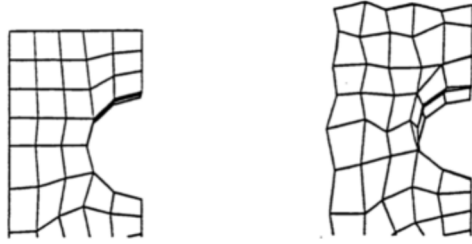

Fig. 10 Stress-strain curve for reinforcing steel

Fig. 11 Undeformed mesh (left) and deformed mesh due to hourglassing (right).

2.4 Hourglass control

Although one-point integration solid and shell elements used in LS-PREPOST LS-DYNA save extensive amounts of simulation time, they are prone to zero-energy modes. For example, if a linear quadrilateral element is estimated using only one integration point at the center of the element for in-plane deformation, then there will be no stiffness present to resist the shear mode which will cause no strain at the center; thus, the strain energy found at the center misses this mode of deformation and the energy of this mode tends to be over-estimated. These spurious modes of deformation, also known as hourglass effects pose the problem of lacking stiffness to resist certain zero-energy modes of deformation. To avoid the zero-energy deformation modes, hourglass control is provided by either viscosity or stiffness added to solid elements. These modes are oscillatory in nature and tend to have periods that are much shorter than those of the overall structural response. Hourglass modes must be effectively controlled or the deformations may grow large and produce an unrealistic geometry. Small damping is usually added into the system to avoid numerical problems. The effects of hourglassing can be seen in Fig. 11. By default, the 8-node solid element uses viscous hourglass. To change default hourglass control type, the Control-Hourglass keyword is used, and the default hourglass control type variable, IHQ, is set to the appropriate type. For solid elements in explicit analysis, the default hourglass control type recommended is stiffness form of type 2 (Flanagan Belytschko), and therefore, IHQ = 4. The energy dissipated by the hourglass forces reacting against the formulations of the hourglass modes is tracked and reported in the output files MATSUM and GLSTAT.

2.5 Body force, dynamic relaxation

Inertial effects are of importance in the simulation of blast loading and material response. Body forces due to inertia effects and all other forces are applied to the structure as dynamic forces due to LS-DYNA explicit solver. To overcome this dilemma, a dynamic relaxation is applied during the duration of unwanted dynamic effects by creating a critically damped dynamic system to rapidly reduce the dynamic effects. At time zero of the simulation, dynamic relaxation is applied for unwanted dynamic effects and until the structure has maintained its natural frequency. Once the structure obtains its natural period, which are approximately 25-45 milliseconds, the dynamic relaxation condition is removed as the blast load is applied.

2.6 Erosion of solid elements

Element erosion is a process which eliminates elements that do not further contribute to resisting the blast loads during the analysis procedure and produce discontinuities in the material due to both brisance effect and fracture induced. With this procedure, it enables the release of adjacent elements to the eliminated one and thus fragments formations occur. Since both of the concrete material models and any other materials in LS-DYNA library do not allow failure and erosion of element, the function Mat Add Erosion is used to account for the deletion of element when a failure criterion is met. In the present study, two failure criteria are used for the concrete material models. They are the minimum pressure at failure (P_{min}) and the maximum principal strain (ε_{max}). Thus, erosion of element will occur either when the pressure experienced by the element, P_1, is lower than the specified minimum pressure or the principal strain ε_1 exceeds the limit maximum principal strain (i.e., $P_1 < P_{min}$ or $\varepsilon_1 > \varepsilon_{max}$). In this investigation, because there is no experimental data available on the tensile strength of the concrete material, the failure pressure was assumed to be the unconfined tensile strength of concrete which was calculated in accordance to the formula proposed by CEB-FIP Model Code (Comite Euro-International du Beton 1990).

$$f'_t = 1.58\left(\frac{(f'_c)^2}{b_0}\right)^{1/3} \tag{8}$$

where f'_t is the unconfined tensile strength of concrete, b_0 is a unit conversion factor (= 145 MPa) and f'_c is the unconfined compressive strength.

3. Blast loads simulation using LaGrangian approach

The Explicit LaGrangian method deals with the observation of stationary particles from the reference viewpoint of a moving particle in terms of material coordinates. The material coordinate labels a material point: each material point has a unique material coordinate, which is usually taken to be its spatial coordinate in the initial configuration of the body. LaGrangian method employs a deformable mesh where nodes and elements move with the material. Typical models are defined to represent deformable structures subjected to dynamic and impulsive loading environments. In general, LaGrangian solutions can be very accurate, economical, and rapid in terms of solution time when applied properly. With careful planning and modeling techniques, complex problems with over 100,000 elements subjected to highly impulsive and short duration environments can be solved accurately using a personal computer in a few hours. The LaGrangian method is typically used for impact and general shock wave propagation problems with limited deformations and mesh distortions. Structural response to impulsive environments is an example of an application well suited for LaGrangian solutions. A schematic representation for the input required for blast generation using the LBE in LS-DYNA is
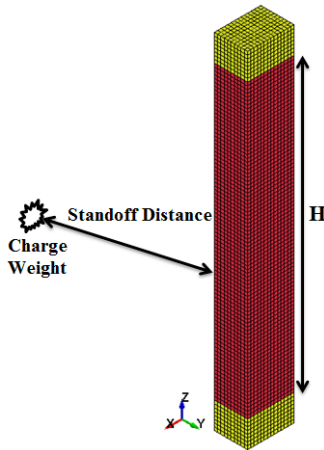
Fig. 12 blast load configurations in the numerical model

Table 2 Material properties of concrete and steel reinforcement (Baylot and Bevins 2007)

Material	Material properties	Value
Concrete	Concrete strength	42 MPa
Main reinforcement	Yield stress	450 MPa
	Ultimate stress	510 MPa
	Fracture strain	18%
Tie bars	Yield stress	400 MPa
	Ultimate stress	610 MPa
	Fracture strain	18%

Fig. 13 Verification of numerical model

in Fig. 12. This approach generally offers simpler application for blast pressure. However, it does not take into account the interaction between air and structure, and therefore the damage mode in close-in detonations may possibly not be captured.

4. Verification of numerical models

Baylot and Bevins (2007) undertook investigations on a quarter-scaled RC two-storey framed building structure subjected to blast loads. The detailed study was confined to the exterior middle columns directly subjected to near-field blast effects. For the validation of the findings from the present analysis, experiment Number 02 of Baylot and Bevins (2007) was selected for the analysis of the behaviour of exterior middle column. The dimensions of the tested column were 85 × 85 × 935 mm. The longitudinal reinforce-ment used was 8D7.1, while the ties were D3.85@102 ties, which were modelled in the numerical analysis and also 8.5 mm mesh size is used in the numerical model.

Gravity load initialization was established prior to blast load application by incorporating a gravitational pressure of 2.1 MPa at the top of the column as a ramped function of time, to represent the self-weight of the frame above the column. The ramped loading was implemented to avoid high stress concentration at the loading zone at the top of the column. Computed blast pressure loads were applied onto the blast-facing surface of the column. Peak pressure and impulse of 7000 kPa and 1100 kPa.ms, respectively, were obtained from the experimental study. The material properties of the concrete and steel reinforcement used in the validation are as shown in Table 2. The comparison of the numerically computed and measured (experimental) deflection-time histories at the middle height of the column is presented in Fig. 13. The maximum lateral displacement measured during the experiment was approximately 12.5 mm, while the displacement computed in the present study was 12 mm with residual displacement of 6.3 mm. The findings obtained in the numerical analysis agree well with the measured deflection-time history. The residual deflection in the present study was also close to those
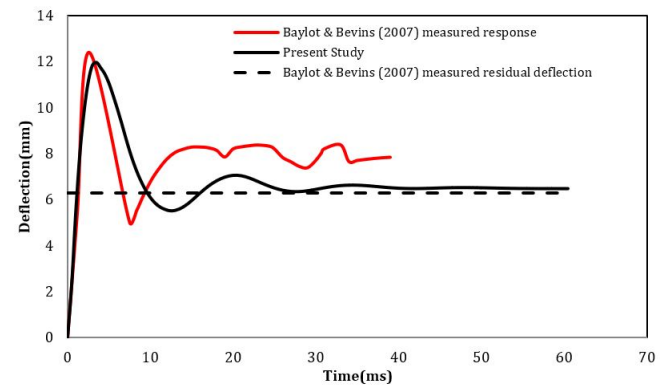
obtained from the experiment.

5. Damage criterion

Each pressure impulse curve represents a damage level that the structural element experiences due to the various blast loading conditions. For this study, the residual axial load carrying capacity is considered as the damage criterion. For each simulation, the residual axial load carrying capacity of the column is read from LS-DYNA's output. After running multiple simulations and following the procedure described above, the points whose damage levels are the same are connected to form a damage level curve, called the pressure impulse diagram for the specific level of structural damage. The damage index in defined as

$$D = 1 - \frac{Presidual}{Pdesign} \qquad (9)$$

Where

➢ $P_{residual}$ = The residual axial load-carrying capacity of the damaged RC column
➢ P_{design} = The maximum axial load carrying capacity of RC column.

The axial load-carrying capacity of an undamaged RC column depends on the longitudinal reinforcement and concrete. According to Macgregor (MacGregor 1996) and ACI Code the following equation is used to assess the maximum axial load-carrying capacity of an undamaged

RC column

$$P_{design} = 0.85 f'_c (A_c - A_s) + f_y A_s \quad\quad (10)$$

Where f'_c is the compressive strength of concrete, f_y the yield strength of the longitudinal reinforcement, A_c gross area of the column cross-section, A_S the area of the longitudinal reinforcement. Damage Index classification shown in Table 3.

Table 3 Damage Index classification

Level of damage	D value
Low damage	0 < D < 0.2
Medium damage	0.2 < D < 0.5
High damage	0.5 < D < 0.8
Collapse	0.8 < D < 1

6. P-I diagrams generation

Numerical simulations were performed to evaluate the dynamic response and to estimate the Pressure-Impulse diagram of the RC columns subjected to explosive loads.

This was followed by an extensive parametric study on the RC columns. The parameters under consideration include column depth, concrete strength, column height and longitudinal reinforcement ratio. While carrying out the parametric studies, other parameters of the RC column remained unchanged. For example, the yield stress of the longitudinal reinforcement bar is 460 MPa, the yield stress of the transverse reinforcement bar is 250 MPa and the uniaxial compressive strength of concrete is 42 MPa. The axial force of the RC column is also considered, which is assumed to be 20% of the column maximum axial load carrying capacity. TNT explosive was used and located at either the middle of the column's height. The ranges of explosive mass are different for all columns and the standoff distance of the charge weight is 1 m from the front
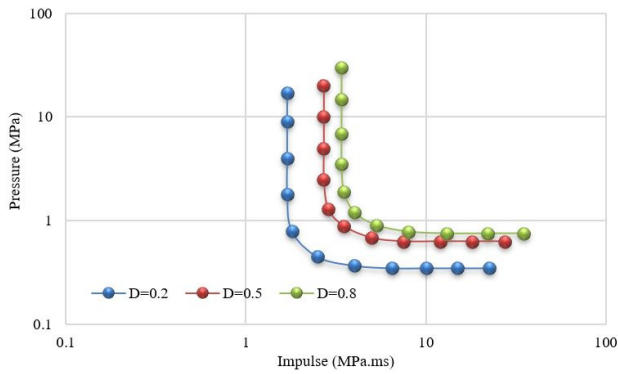
Column C1
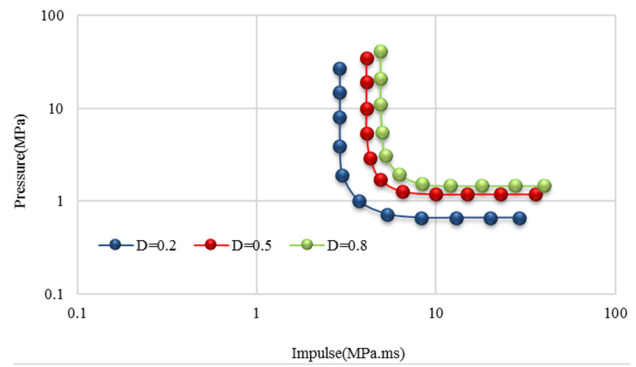
Column C2
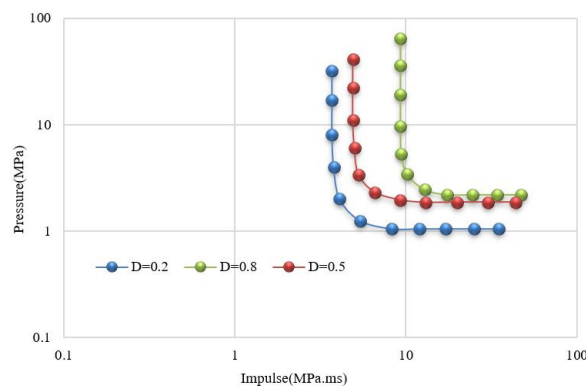
Column C3

Fig. 14 P-I models generation for columns C1, C2 & C3

Table 4 The configuration of the RC columns

Column no.	Column width (mm)	Column depth (mm)	Column height (mm)	Cross tie/hoop	Longitudinal reinforcement
C$_1$	500	700	4400	D12@200	8D25
C$_2$	700	700	4400	D12@200	8D25
C$_3$	700	900	4400	D12@200	8D25

face of the RC columns. Fig. 14 shows the pressure–impulse diagram of RC columns C1, C2 and C3 derived from the curve-fitting method. The configuration of the columns is given in Table 4.

7. Analytical formulae to generate P–I diagram

Analytical formulae are generated for predicting the pressure asymptote and impulsive asymptote of the RC column under blast loads. The prediction is based on the

results of the parametric studies. The formulae of the pressure asymptote and impulsive asymptote of the RC columns are as follows (FACEDAP 1994)

$$(P - P_0)(I - I_0) = 3\left(\frac{P_0}{2} + \frac{I_0}{2}\right)^{1.5} \tag{11}$$

Where $P_0(MPa)$ is the pressure asymptote and $I_0(MPa)$ is the impulsive asymptote. The best fitted P–I curve of RC column according to Eq. (11) were plotted in Fig. 15 for different damage levels. This demonstrated that
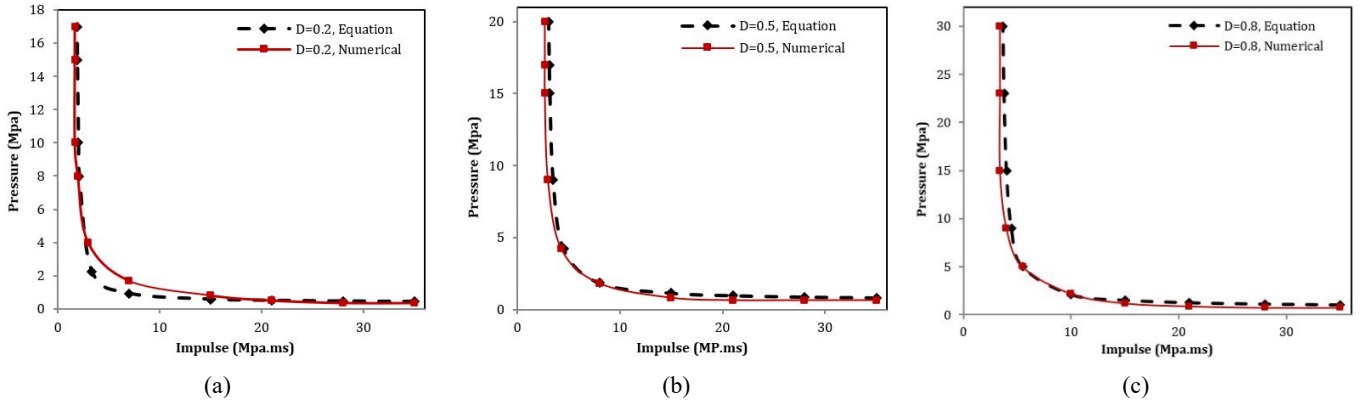

(a)   (b)   (c)

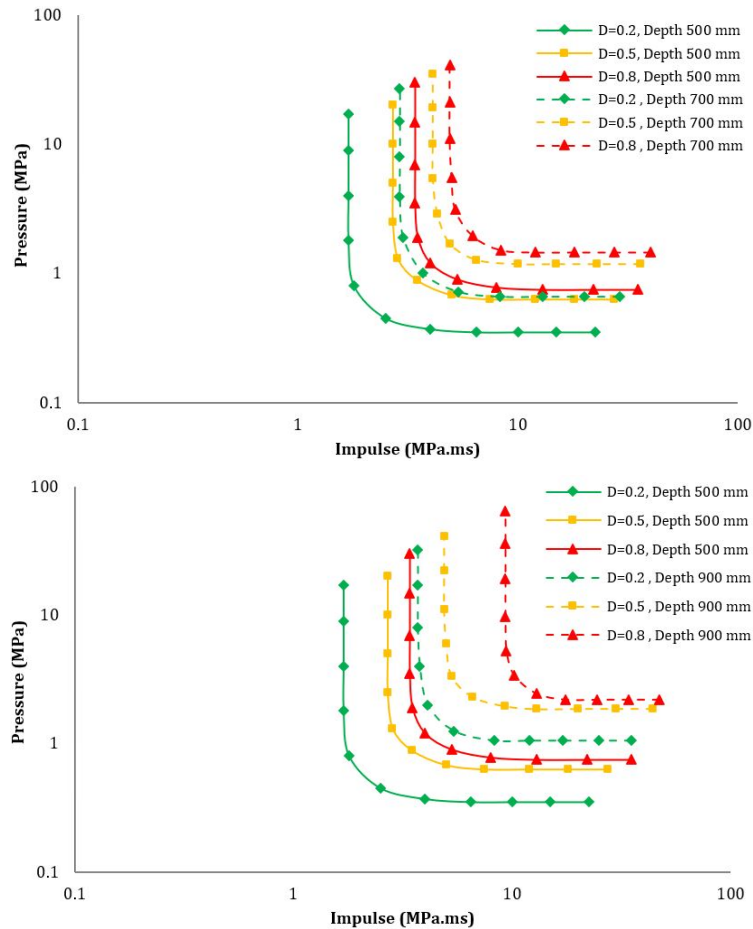Fig. 15 P-I diagram generated from Eq. (11) and numerical data for column C2

Fig. 16 P-I model for RC columns with various *d*

Eq. (11) could be used to model P–I diagram for the RC columns with different damage levels. As can be shown in Fig. 15, the fitted curve which is generated by Eq. (11) is similar to the points generated by the numerical method.

8. Results and discussion

8.1 Effect of column depth, *d*

To investigate the influence of the *d* on the RC column P-I model under explosive loads, three different column depths, namely 500, 700 and 900 mm are studied. The yield stress of the longitudinal reinforcement bar is 460 MPa, the yield stress of the transverse reinforcement bar is 250 MPa and the uniaxial compressive strength of concrete is 42 MPa. The column width, column height, transverse reinforcement ratio, longitudinal reinforcement ratio and steel strength of the three columns are the same in all columns. the effect of column depth on the RC column pressure–impulse diagram shown in Fig. 16. As can be seen from Fig. 16, the both the pressure asymptote and impulsive asymptote of the RC column increase significantly with the increase in column depth. It can be observed that columns with bigger depth show increased resistance to failure under explosive loads. An increase in column depth results in more concrete area and a larger cross section modulus,

which in turn improves both shear and bending strength of the column.

8.2 Effects of Column height, H

In this section, the influence of column height on the behaviour of columns exposed to severe condition events is studied. The range of column height is chosen between 3400 mm and 5400 mm to consider the influence of column height on the RC column resistance against blast load while the column depth and column width as well as the ρ are constant for the three RC columns. As can be shown in Fig. 17, with the increased column height, the pressure and impulse asymptotes of RC column can be decreased. From the results, it is apparent that increase the column height results in a decrease in the column blast load-carrying capacity, especially the flexural resistance capacity as evidenced by the reduction in the pressure asymptote. Increasing the column height results in an increase in the bending moment acting on the column therefore reduce the pressure asymptote since the column cross section is a constant.

8.3 Effects of Concrete Strength, f_c

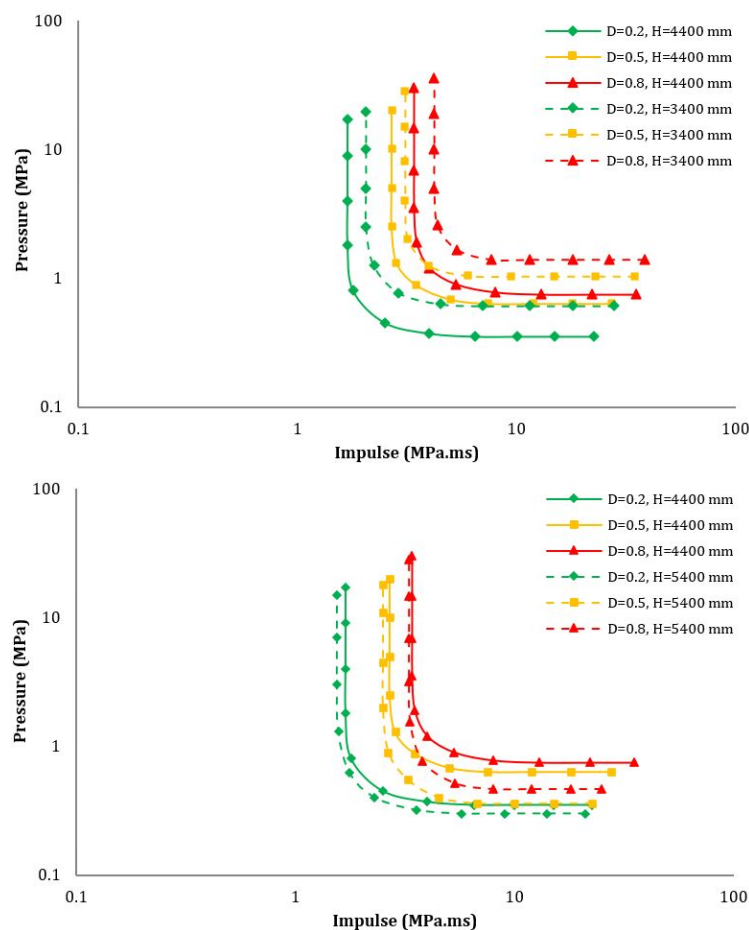It seems that the concrete strength might be another important factor on the damage rate of the column.

Fig. 17 P-I model for RC columns with various *H*

Columns with concrete strength of 32, 42 and 52 MPa were analyzed to generate the corresponding P–I diagram. The comparisons of the simulated pressure and impulse asymptotes of the P-I curves of RC column with different concrete strength are shown in Fig. 18. The results indicate that the damage level of columns decreases by increasing the column strength under the same scaled distance. Meanwhile, columns with higher compressive strength provide higher failure resistance under blast loads; which is due to the fact that the f_c is related to the shear and bending strength of the column simultaneously. It was shown that increasing the concrete strength would increase both the pressure and the impulsive asymptote of the flexure and shear P-I curve.

8.4 Effect of longitudinal reinforcement ratio (ρ)

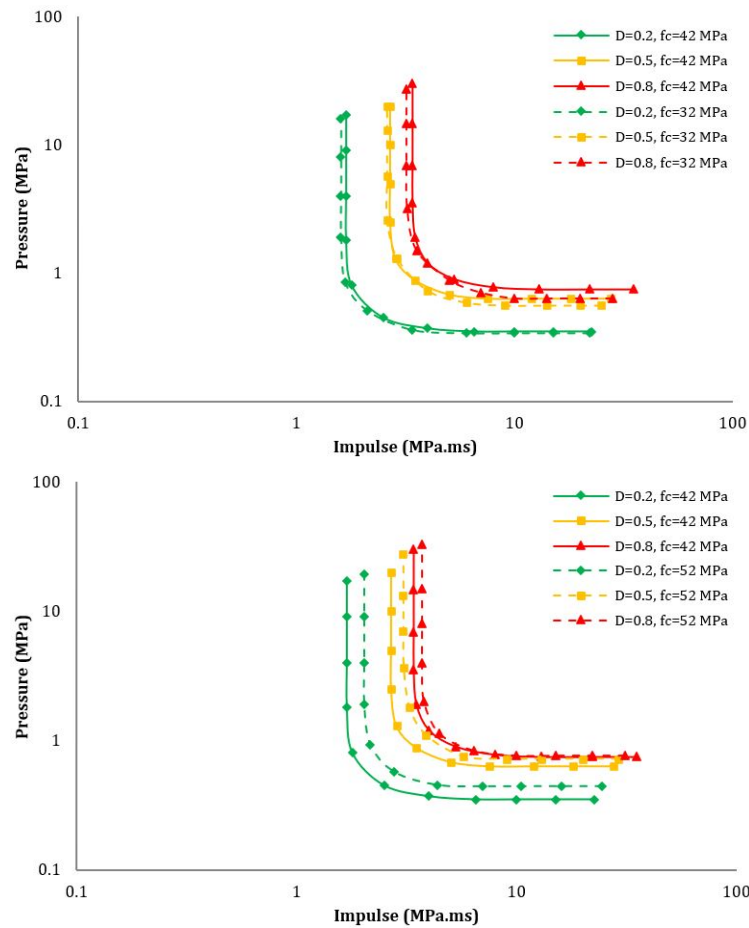In the current section, the ρ for three different columns

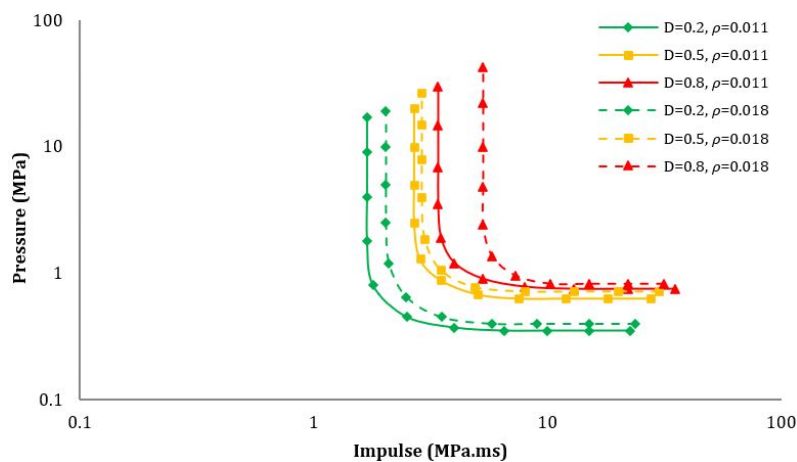Fig. 18 P-I model for RC columns with various f_c

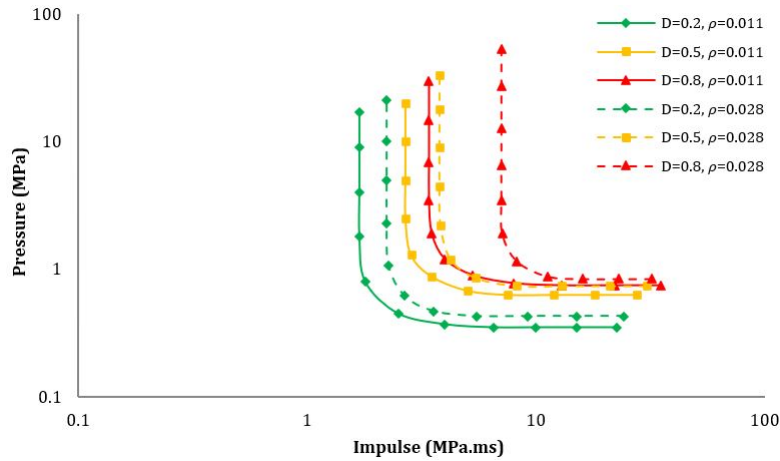Fig. 19 P-I model for RC columns with various ρ
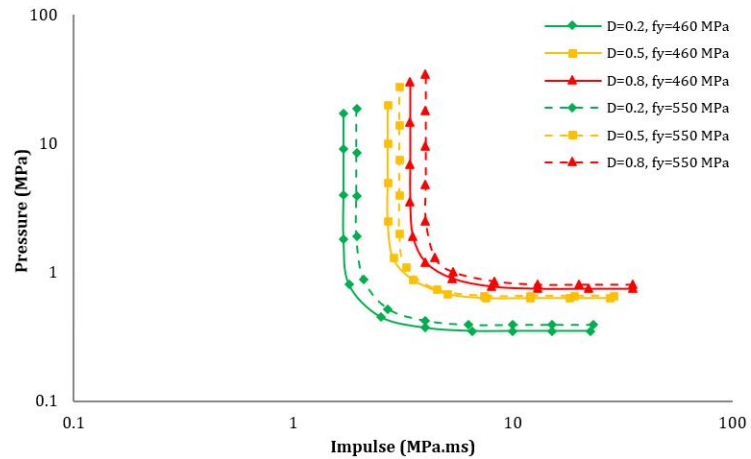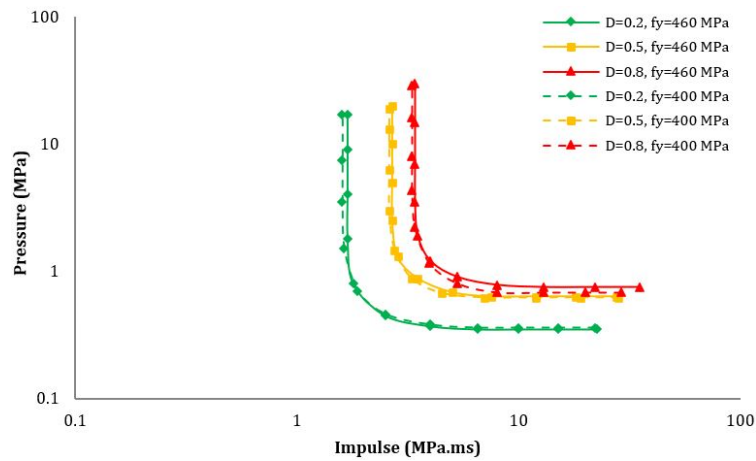
Fig. 19 Continued

Fig. 20 P-I model for RC columns with various f_y

is considered. Various ρ i.e., 0.011, 0.018 and 0.028 are obtained through modifying the main rebar diameter while the column dimension and the transverse reinforcement ratio kept unchanged for another columns. The main bar diameters used for the three columns are 25, 32 and 40 mm.

Fig. 19 shows the comparison of different longitudinal reinforcement ratio on the pressure-impulse diagram of the blast-damaged columns. The results indicate that when the

ρ increases, the damage will decrease effectively by increasing the scaled distance. This behavior can be attributed to the enhancement in the bending strength of the column by increasing the ρ; however, it has negligible contribution to the shear strength. As can be noted, the impulsive asymptotes of the RC columns increase with the reinforcement ratio and the impulsive asymptotes has larger increment than the pressure asymptotes, indicating the

reinforcement has more significant effect on flexural than shear resistance capacity of the columns. In most cases the column collapse is related to the increase of axial load carried by the longitudinal reinforcing bars up till the complete deterioration of its compressive strength carrying capacity. An increase in longitudinal reinforcement ratio provides additional axial load carrying capacity to the column and only limited contribution to its shear strength.

8.5 Effect of longitudinal Steel strength, f_y

Besides the column dimensions, the longitudinal steel strength might have a significant influence on the pressure asymptotes and impulsive asymptotes of the P–I curve of the RC column. The steel strength of the three column varies from 400 MPa to 550 MPa while the transverse steel strength is unchanged in all three columns. Column depth was 500 mm, the width was 700 mm, the height was 4400 mm and the concrete strength was 42 MPa. The comparisons of the simulated pressure and impulse asymptotes of the P-I curves of RC column with different concrete strength are shown in Fig. 20. It can be concluded therefore that the stronger longitudinal steel strength improves the RC columns shear strength. The results show that the influence of the longitudinal steel strength on the blast-resistance performance of RC columns against close-in explosions is obvious.

9. Conclusions

In the current study, Pressure-Impulse diagram for RC columns under explosive loads developed by using finite element analysis. The analysis was performed using LS-DYNA non-linear explicit FE code. The accuracy of the numerical models was verified using the findings of experimental data obtained by other researchers. The verified models were then used to simulate behavior of RC column to blast loads. Parametric studies were conducted to investigate the effects on P-I curves of changing several parameters, including column depth, column height, reinforcement ratio, concrete strength and steel strength. The results show that the bigger depth is most strongly resist blast loading because of their high energy absorption capacity. An increase of the longitudinal reinforcement ratio can cause significant increase in the pressure asymptotes and impulsive asymptotes of the P-I curve of RC columns. A column with shorter height can decrease the damage due to explosive load and finally a column with higher longitudinal steel strength can retain more blast load. This study illustrates that pressure-impulse diagrams developed by using the results of finite element analysis are capable of capturing the reduction of damage level caused by changes in the different parameters.

Acknowledgments

References

Abedini, M. and Zhang, C. (2021a), "Dynamic vulnerability assessment and damage prediction of RC columns subjected to severe impulsive loading", *Struct. Eng. Mech.*, *Int. J.*, **77**(4), 441-461. https://doi.org/10.12989/sem.2021.77.4.441

Abedini, M. and Zhang, C. (2021b), "Performance assessment of concrete and steel material models in ls-dyna for enhanced numerical simulation, a state of the art review", *Archives Computat. Methods Eng.*, **28**(4), 2921-2942. https://doi.org/10.1007/s11831-020-09483-5

Abedini, M. and Zhang, C. (2021c), "Dynamic performance of concrete columns retrofitted with FRP using segment pressure technique", *Compos. Struct.*, **260**, 113473. https://doi.org/10.1016/j.compstruct.2020.113473

Abrahamson, G.R. and Lindberg, H.E. (1976), "Peak load-impulse characterization of critical pulse loads in structural dynamics", *Nuclear Eng. Des.*, **37**, 35-46. https://doi.org/10.1016/0029-5493(76)90051-0

Alipour, R., Izman, S. and Tamin, M.N. (2014), "Estimation of charge mass for high speed forming of circular plates using energy method", *Adv. Mater. Res.*, **845**, 803-808. https://doi.org/10.4028/www.scientific.net/AMR.845.803

Alipour, R., Frokhi Nejad, A., Izman, S. and Tamin, M. (2015), "Computer aided design and analysis of conical forming dies subjected to blast load", *Appl. Mech. Mater.*, **735**, 50-56. https://doi.org/10.4028/www.scientific.net/AMM.735.50

Baylot, J.T. and Bevins, T.L. (2007), "Effect of responding and failing structural components on the airblast pressures and loads on and inside of the structure", *Comput. Struct.*, **85**(11), 891-910. https://doi.org/10.1016/j.compstruc.2007.01.001

Comite Euro-International du Beton (1990), "Concrete structures under impact and impulsive loading", CEB Bulletin, N°187.

Cormie, D., Mays, C. and Smith, P. (2009), *Blast Effects on Buildings*, (2nd Edition), Thomas Telford Ltd., London, UK.

Dragos, J. and Wu, C. (2013), "A new general approach to derive normalised pressure impulse curves", *Int. J. Impact Eng.*, **62**, 1-12. http://dx.doi.org/10.1016/j.ijimpeng.2013.05.005

FACEDAP (1994), Facility and component explosive damage asessment program, In: SwRI Project No.06-5145-001; U.S. Army Corps of Engineers, Omaha District, Omaha, NE, USA.

Gang, H. and Kwak, H.-G. (2017), "A tensile criterion to minimize FE mesh-dependency in concrete beams under blast loading", *Comput. Concrete*, *Int. J.*, **20**(1), 1-10. https://doi.org/10.12989/cac.2017.20.1.001

Govindjee, S., Kay, G.J. and Simo, J.C. (1995), "Anisotropic modelling and numerical simulation of brittle damage in concrete", *Int. J. Numer. Methods. Eng.*, **38**(21), 3611-3633. https://doi.org/10.1002/nme.1620382105

Hadianfard, M.A. and Farahani, A. (2012), "On the effect of steel columns cross sectional properties on the behaviours when subjected to blast loading", *Struct. Eng. Mech.*, *Int. J.*, **44**(4), 449-463. http://doi.org/10.12989/sem.2012.44.4.449

Izman, S., Nejad, A.F., Alipour, R., Tamin, M. and Najarian, F. (2015), "Topology optimization of an asymmetric elliptical cone subjected to blast loading", *Procedia Manuf.*, **2**, 319-324. https://doi.org/10.1016/j.promfg.2015.07.056

Jain, P. and Chakraborty, T. (2018), "Numerical analysis of tunnel in rock with basalt fiber reinforced concrete lining subjected to

internal blast load", *Comput. Concrete, Int. J.*, **21**(4), 399-406.
https://doi.org/10.12989/cac.2018.21.4.399

Kim, D.K., Ng, W.C.K. and Hwang, O. (2018), "An empirical formulation to predict maximum deformation of blast wall under explosion", *Struct. Eng. Mech., Int. J.*, **68**(2), 237-245.
https://doi.org/10.12989/sem.2018.68.2.237

Li, Q. and Meng, H. (2002), "Pressure-impulse diagram for blast loads based on dimensional analysis and single-degree-of-freedom model", *J. Eng. Mech.*, **128**(1), 87-92.
https://doi.org/10.1061/(ASCE)0733-9399(2002)128:1(87)

LS-DYNA (2007), LS-DYNA Version 970 Keyword User's Manual: Livermore Software Technology Corporation.

Lu, Y. and Xu, K. (2004), "Modelling of dynamic behaviour of concrete materials under blast loading", *Int. J. Solids Struct.*, **41**(1), 131-143. https://doi.org/10.1016/j.ijsolstr.2003.09.019

MacGregor, J. (1996), *Reinforced concrete*: *mechanics and design. Professional technical reference*, Prentice-Hall, Englewood Cliffs, NJ, USA.

Mahdavi, N., Ahmadi, H.R. and Bayat, M. (2019), "Efficient parameters to predict the nonlinear behavior of FRP retrofitted RC columns", *Struct. Eng. Mech., Int. J.*, **70**(6), 703-710.
https://doi.org/10.12989/sem.2019.70.6.703

Malvar, L.J. (1998), "Review of static and dynamic properties of steel reinforcing bars", *ACI Mater. J.*, **95**(5), 609-616.

Malvar, L.J., Crawford, J.E., Wesevich, J.W. and Simons, D (1997), "A plasticity concrete material model for DYNA3D", *Int. J. Impact Eng.*, **19**(9), 847-873.
https://doi.org/10.1016/S0734-743X(97)00023-7

Pandey, A. (2010), "Damage prediction of RC containment shell under impact and blast loading", *Struct. Eng. Mech., Int. J.*, **36**(6), 729-744. http://doi.org/10.12989/sem.2010.36.6.729

Rashad, M. and Yang, T. (2019), "Improved nonlinear modelling approach of simply supported PC slab under free blast load using RHT model", *Comput. Concrete, Int. J.*, **23**(2), 121-131.
https://doi.org/10.12989/cac.2019.23.2.121

Rezaei, M.J., Gerdooei, M. and Nosrati, H.G. (2020), "Blast resistance of a ceramic-metal armour subjected to air explosion: A parametric study", *Struct. Eng. Mech., Int. J.*, **74**(6), 737-745.
https://doi.org/10.12989/sem.2020.74.6.737

Thiagarajan, G., Rahimzadeh, R. and Kundu, A. (2013), "Study of pressure-impulse diagrams for reinforced concrete columns using finite element analysis", *Int. J. Protect. Struct*, **4**(4), 485-504. https://doi.org/10.1260/2041-4196.4.4.485

Wang, Z.L., Wang, J.G., Li, Y.C. and Leung, C.F. (2006), "Attenuation effect of artificial cavity on air-blast waves in an intelligent defense layer", *Comput. Geotech.*, **33**(2), 132-141.
https://doi.org/10.1016/j.compgeo.2006.02.002

Zhang, C. and Abedini, M. (2021), "Time-history blast response and failure mechanism of RC columns using Lagrangian formulation", *Structures*, **34**, 3087-3098.
https://doi.org/10.1016/j.istruc.2021.09.073

Zhang, C. and Abedini, M. (2022), "Development of PI model for FRP composite retrofitted RC columns subjected to high strain rate loads using LBE function", *Eng. Struct.*, **252**, 113580.
https://doi.org/10.1016/j.engstruct.2021.113580

Zhang, Y., Zhao, K., Li, Y., Gu, J., Ye, Z. and Ma, J. (2018), "Study on the local damage of SFRC with different fraction under contact blast loading", *Comput. Concrete, Int. J.*, **22**(1), 63-70. https://doi.org/10.12989/cac.2018.22.1.063

Zhang, C., Abedini, M. and Mehrmashhadi, J. (2020), "Development of pressure-impulse models and residual capacity assessment of RC columns using high fidelity Arbitrary Lagrangian-Eulerian simulation", *Eng. Struct.*, **224**, 111219.
https://doi.org/10.1016/j.engstruct.2020.111219

JK